Dynamical Analysis of Neural Oscillators in an Olfactory Cortex Model

Dongming Xu, *Student Member, IEEE,* and José C. Principe, *Fellow, IEEE*

***Abstract*—This paper presents a theoretical approach to understand the basic dynamics of a hierarchical and realistic computational model of the olfactory system proposed by W. J. Freeman. While the system's parameter space could be scanned to obtain the desired dynamical behavior, our approach exploits the hierarchical organization and focuses on understanding the simplest building block of this highly connected network. Based on bifurcation analysis, we obtain analytical solutions of how to control the qualitative behavior of a reduced KII set taking into consideration both the internal coupling coefficients and the external stimulus. This also provides useful insights for investigating higher level structures that are composed of the same basic structure. Experimental results are presented to verify our theoretical analysis.**

***Index Terms*—Bifurcation, differential equations, nonlinear oscillators, olfactory system, stability.**

I. Introduction

A REALISTIC computational model of the olfactory system proposed by Freeman describes brain function as a spatio-temporal lattice of groups of neurons (neural assemblies) with dense interconnectivity [1]. Generally, a Nth-order system is defined by

$$\frac{1}{a\cdot b}\cdot\left[\frac{\mathrm{d}^2x_i(t)}{\mathrm{d}t^2}+(a+b)\cdot\frac{\mathrm{d}x_i(t)}{\mathrm{d}t}+(a\cdot b)\cdot x_i(t)\right]$$
$$=\sum_{j\neq i}^{N}\left[W_{ij}\cdot Q\left(x_j(t),Q_m\right)+W'_{ij}\cdot f_j\left(Q\left(x_j(t),Q_m\right),t\right)\right]$$
$$+P_i(t)\quad i=1,\ldots,N \tag{1}$$

where $1/a$ and $1/b$ are time constants that define the second-order dynamics. Each processing element (PE) in (1) models the independent dynamics of the wave density for the action dendrites and the pulse density for the parallel action of axons. Note that there is no auto-feedback in the model. $Q(x)$ is the asymmetric nonlinear function (at the output stage) in each PE, and it describes the wave to pulse transformation. The mathematical model and properties of $Q(x)$ will be discussed later in this paper. Freeman's model is a locally stable and globally unstable dynamical system in a very high-dimensional space. In spite of its complexity, the model is built from a hierarchical embedding of simpler and similar structures. Based on the seminal work of Katchalsky [1], four different levels named K0, KI, KII, and KIII are included in the model, and are defined as follows [1], [2].

K0 The K0 set is the most basic and simplest building block in the hierarchy. All higher level structures are made of interconnected K0 sets. The K0 includes three stages, as illustrated in Fig. 1. Spatial inputs to a K0 set are weighted and summed. And the resulting signal is passed through a linear time-invariant system with second-order dynamics. The output of the linear system is shaped by the asymmetric nonlinear function $Q(x)$. Two categories of K0 sets (excitatory and inhibitory) are defined by the sign of the nonlinear function. There is no coupling among the K0 sets when forming a K0 network.

KI K0 sets with common sign (either excitatory or inhibitory) are connected through forward lateral feedback to construct a KI network. No auto-feedback is allowed in the network.

KII A KII set in the model is a coupled oscillator that consists of two KI sets (or four K0 sets). Each set has fixed coupling coefficients obtained from biological experiments. A KII set is the basic computational element in Freeman's olfactory system. The measured output from any of the nonlinear functions has two stable states that are controlled by the external stimulus. The resting state occurs when external input is in the zero state while an oscillation occurs when the external input is present. Therefore a KII set is an oscillator controlled by the input. The KII network is built from KII sets interconnected with both the excitatory cells (denoted by M1) and inhibitory cells (G1). This interconnected structure represents a key stage of learning and memory in the olfactory system. Input patterns through M1 cells are mapped into spatially distributed outputs. Excitatory and inhibitory interconnections enable cooperative and competitive behaviors, respectively, in this network. The KII network functions as an encoder of input signals or as an auto-associative memory [1], [2].

KIII The KIII network embodies the computational model of the olfactory system. It has different layers representing anatomical regions of a mammalian brain. In a KIII network, basic KII sets and a KII network are tightly coupled through dispersive connections (mimicking the different lengths and

Manuscript received May 27, 2003; revised December 13, 2003. This work was partially supported by the Office of Naval Research under Grant N00014-1-1-0405.

The authors are with the Computational NeuroEngineering Laboratory, Department of Electrical and Computer Engineering, University of Florida, Gainesville, FL 32611 USA (dmxu@cnel.ufl.edu; principe@cnel.ufl.edu).

Digital Object Identifier 10.1109/TNN.2004.832815

thicknesses of nerve bundles). Since the intrinsic oscillating frequencies of each one of the KII sets in different layers are incommensurate among themselves, this network of coupled oscillators will present chaotic behavior.

Freeman's model quantifies the function of one of the oldest sensory cortices, where there is an established causal relation between stimulus and response. It also presents the function as an association between stimulus and stored information, in line with the auto-content addressable memory (CAM) framework studied in artificial neural networks [3]. Freeman utilizes the language of dynamics to model neural assemblies, which seems a natural solution due to the known spatio-temporal characteristics of brain function [4]. Although we believe that the full dynamical description of the KIII network is beyond our present analytical ability, one may still be able to understand the dynamics of the KII network from first principles. One of the advantages of a dynamical framework to quantify mesoscopic interactions is related to the possibility of creating analog VLSI circuits that implement similar dynamics [2], [5]. In this respect, dynamics are also independent of the hardware, mimicking the well known hardware independence characteristics of formal systems. However, the dynamical approach to information processing is much less developed when compared with the statistical reasoning used in pattern recognition. Only recently were nonlinear dynamics used to describe computation [6] and a nonlinear dynamical theory of information processing is still an illusory goal. Hence, we are at the same time developing the science and understanding the tool capabilities, which is far from the ideal situation. The challenge is particularly important in the case of Freeman's model, where the distributed system is locally stable but globally unstable, creating nonconvergent (eventually chaotic) dynamics. Nonconvergent dynamics are very different from the simple dynamical systems with point attractors studied by Hopfield [7], because they have positive Lyapunov exponents [8]. Freeman's computational model of olfactory system has already been applied to several information processing application [2], [5], [9], [10]. Ultimately, we plan to use Freeman's model as a signal to symbol translator, quantify its performance and implement them in analog VLSI circuits for low power, real time processing in intelligent sensory processing applications.

To accomplish the tasks mentioned above. It is of great interest to understand the dynamical behavior of this system, starting from the most basic elements. For example, in hardware designs, variations in design processes and fabrication as well as noise may degrade the performance of the system. We want to quantify the sensitivity of the key parameters in the model and make sure that noise and errors could not significantly change the dynamical system behavior. From the information processing point of view, we want to make sure each PE remains in the appropriate dynamic regime and does not generate complicated behavior. On the other hand, evaluating specific properties of the network could also help us choose the best way to use it. Bifurcation analysis of several oscillatory neural networks constructed from KI set are discussed in [11]. Numerical approaches are used to obtain the bifurcation diagram of those networks. In this paper, we will perform bifurcation analysis in a theoretical way and focus on the dynamical behaviors of the reduced KII (RKII) set, which is a simplified version of the KII set. Section II-A gives a brief review of the techniques needed to analyze the system. The rest of Section II presents a RKII set as a nonlinear dynamical system and investigates its qualitative dynamic behavior. Conditions on control parameters such as the coupling coefficients and external stimulus are discussed. Section III gives the experimental results that verify the theoretical analysis given in Section II. The main conclusions are summarized in Section IV.

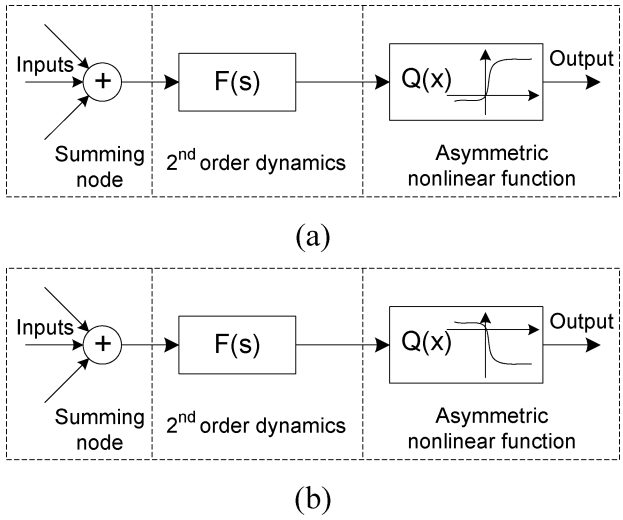

Fig. 1. Diagram of K0 sets. (a) An excitatory K0 set. (b) An inhibitory K0 set.

II. Bifurcation Analysis of RKII Sets in the Olfactory Model

A. Nonlinear Dynamic Systems Analysis

A linear time-invariant system is defined as

$$\frac{\mathrm{d}x}{\mathrm{d}t} = A \cdot x(t) \tag{2}$$

where $x \in R^N$. $A \in R^{N \times N}$ is a constant matrix.

The qualitative behavior of (2) is determined by the eigenvalues of A. The solution $x(t) = x(0) \cdot e^{A \cdot t}$ may have the following possible dynamical behaviors:

1) The system has a fixed point solution if the real parts of all the eigenvalues of A are negative;
2) The system is unstable if at least one of the eigenvalues of A has positive real part.
3) In the case that all eigenvalues of A have a real part that is less than or equal to zero, if all eigenvectors corresponding to the eigenvalues with zero real part are independent, the system is stable, otherwise it is unstable.

We see that the analysis of a linear system is rather simple and straightforward since all dynamics are clearly determined by the eigenvalues of A. For a nonlinear system, more complicated behaviors may exist. In most cases, a nonlinear system is linearized around its equilibrium so that an explicit solution and qualitative analysis could be achieved around the neighborhood of the equilibrium points [12]. The conditions that guarantee a qualitatively similar phase portrait between a nonlinear system

and its linearized version is described by the Hartman-Grobman Theorem [13]. According to the theorem, a nonlinear system

$$\frac{\mathrm{d}x}{\mathrm{d}t} = f(x) \tag{3}$$

is locally topologically equivalent (preserving the parameterization) to its linearization as defined in (2) (that is, there is a homeomorphism in a neighborhood of the equilibrium that maps orbits of the nonlinear to the linear flows.), if the linearization $A(x_0)$ has no purely imaginary eigenvalues. In this case, this nonlinear system is a locally hyperbolic dynamical system.

Thus, the stability analysis of a nonlinear system could be greatly simplified while preserving qualitative properties. Of course, this happens when the system is not at a bifurcation point [13]. Bifurcation occurs when a system is structurally different with respect to the variation of its parameter set. A parameter-dependent system may present different behavior in phase space when the parameter passes through a certain point called a bifurcation point [13]. While bifurcation analysis is important to understand complex systems, in this paper, we will use it to guarantee that the system behavior remains basically unchanged in the neighborhood of the operating point. For a simple 2-dimensional planar system, the Poincaré-Bendixon theorem gives more information about the exact system state [12], [14], [15].

Consider a second-order autonomous dynamical system in the following form:

$$\begin{cases} \dot{x} = f(x,y) \\ \dot{y} = g(x,y). \end{cases} \tag{4}$$

Let D be a closed and bounded region in R^2 containing a finite number of equilibrium points of (4). A solution of (4) remains entirely in D. Then, based on the Poincaré-Bendixon theorem, the solution has three possible behaviors: 1) it approaches an equilibrium point; 2) it approaches a closed path; 3) the solution is a union of saddles and their connections. Note that the Poincaré-Bendixon theorem deals only with a 2-dimensional system and it does not generalize to higher order systems. In the following sections, we will utilize these concepts to analyze the qualitative behavior of a RKII set. From experimental observations, we will propose a hypothesis that uses the same concept as the Poincaré–Bendixon theorem but can be applied to our fourth-order system.

B. Dynamics of a RKII Set

A RKII set is a simplified version of the KII set [5]. Instead of having four PEs (two excitatory K0 sets and two inhibitory K0 sets) in the set, it only has one excitatory (mitral) and one inhibitory (granule) PE (Fig. 2). The M and G PEs are coupled by two coupling coefficients K_{mg} and K_{gm}. $P(t)$ is the external stimulus. In this paper, we will only consider a time-invariant input. That is, $P(t)$ will only have either *off* or *on* state that represents zero or positive input, respectively. In a KII network with large number of channels, the KII set can be replaced by the RKII set [5]. Because of its simplicity, we start our analysis from the RKII set and hope to understand higher level structures by investigating the dynamical behavior of this

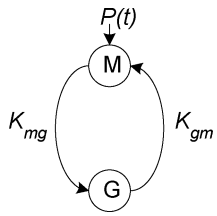

Fig. 2. RKII set consists of one mitral PE and one granule PE that are coupled through $K_{mg}(>0)$ and $K_{gm}(<0)$.

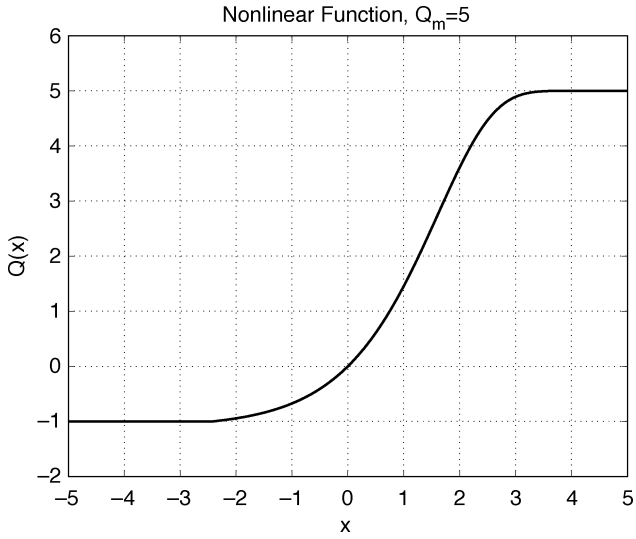

Fig. 3. Plot of the nonlinear function $Q(x)$ defined by (6) when $Q_m = 5$.

basic building block. A RKII set is described by the following system of second-order ordinary differential equations (ODEs):

$$\begin{cases} \frac{1}{a\cdot b}\cdot\left(\frac{\mathrm{d}^2 m(t)}{\mathrm{d}t^2} + (a+b)\cdot\frac{\mathrm{d}m(t)}{\mathrm{d}t} + m(t)\right) \\ \quad = K_{gm}Q(g) + P & K_{gm} < 0 \\ \frac{1}{a\cdot b}\cdot\left(\frac{\mathrm{d}^2 g(t)}{\mathrm{d}t^2} + (a+b)\cdot\frac{\mathrm{d}g(t)}{\mathrm{d}t} + g(t)\right) \\ \quad = K_{mg}Q(m) & K_{mg} > 0. \end{cases} \tag{5}$$

$1/a$ and $1/b$ are time constants of the second-order dynamics. They are given experimentally as $a = 220/s$ and $b = 720/s$ [1]. $Q(x)$ is the nonlinear function that models the spatio-temporal integration of spikes into mesoscopic waves measured in the cortex [1] and is defined by

$$Q(x) = \begin{cases} Q_m \cdot \left(1 - e^{-\frac{e^x - 1}{Q_m}}\right) & x > x_0 \quad \text{(6a)} \\ -1 & \text{else} \quad \text{(6b)} \end{cases}$$

where $x_0 = \ln(1 - Q_m \cdot \ln(1 + 1/Q_m))$. Q_m is an adjustable parameter that controls the ratio between positive and negative saturation values of $Q(x)$ (Fig. 3). In this paper, we only use (6a) for all x. The discontinuity should not change the results we obtain here. Simulation results in Section III will verify all the analysis.

In simulations, we observe as predicted that a RKII set only has two stable behaviors: a fixed point or a limit cycle. In the following we will give the analytical solution of how the internal coupling coefficients determine the dynamical behavior of (5). This is achieved by computing the real part of the eigenvalues of the system's Jacobian matrix. Their signs indicate the state

of the RKII set. The analysis helps avoid bifurcation regions in the parameter space and guarantee simple dynamics.

C. Bifurcation Analysis of a RKII Set

Using proper substitutions, we could rewrite (5) as

$$\begin{cases} \dfrac{\mathrm{d}m_1(t)}{\mathrm{d}t} = m_2 \\ \dfrac{\mathrm{d}m_2(t)}{\mathrm{d}t} = -ab \cdot m_1 - (a+b) \cdot m_2 + ab \cdot (K_{gm}Q(g_1) + P) \\ \dfrac{\mathrm{d}g_1(t)}{\mathrm{d}t} = g_2 \\ \dfrac{\mathrm{d}g_2(t)}{\mathrm{d}t} = -ab \cdot g_1 - (a+b) \cdot g_2 + ab \cdot K_{mg}Q(m_1). \end{cases} \tag{7}$$

As stated in the Hartman–Grobman theorem, a nonlinear system is topologically equivalent to its linearization around equilibrium if the linearization has no purely imaginary eigenvalues. In this case, if we set K_{mg} and K_{gm} so that (7) is a locally hyperbolic system, the dynamical behavior then becomes a stability analysis at equilibrium. In our case, the equilibrium will be either stable or unstable based on the sign of the real part of eigenvalues computed from the Jacobian matrix. With a stable equilibrium, we expect the system to converge to a fixed point from any initial condition. If the equilibrium is unstable, we know that any deviation from it will diverge. However, the system is bounded thanks to the nonlinear function $Q(x)$. According to the Poincaré-Bendixon theorem, if the system is 2-dimensional, the solution in this case should be a limit cycle. Although without proof, here we also expect our system to approach a limit cycle and give the following hypothesis:

Hypothesis: Assume that a RKII set is not at a bifurcation point, then its dynamical behavior is determined by the qualitative behavior at its equilibrium points. More specifically, if the equilibrium point is stable, the solution of a RKII set will approach a fixed point; if the equilibrium is unstable, the solution of a RKII set will approach a stable limit cycle.

The equilibrium can not be solved analytically, but a numerical solution and properties of the equilibrium will be pursued below. First, we will see that this system has a unique equilibrium. Let us assume m_1^* and g_1^* are the state variables of (7) at equilibrium. (8) gives the equations that determine the equilibrium. As shown in Fig. 4, the equilibrium should be the intersections of the two nullclines defined as

$$\begin{cases} -ab \cdot m_1^* + ab \cdot (K_{gm}Q(g_1^*) + P) = 0 \\ -ab \cdot g_1^* + ab \cdot K_{mg}Q(m_1^*) = 0. \end{cases} \tag{8}$$

The following gives some of the properties of the equilibrium of (7):

Property 1: Assume that $K_{mg} > 0$, $K_{gm} < 0$ and $P \geq 0$, there is one and only one equilibrium in a RKII set defined by (7). The equilibrium is always in the first quadrant, i.e., $m_1^* \geq 0$ and $g_1^* \geq 0$.

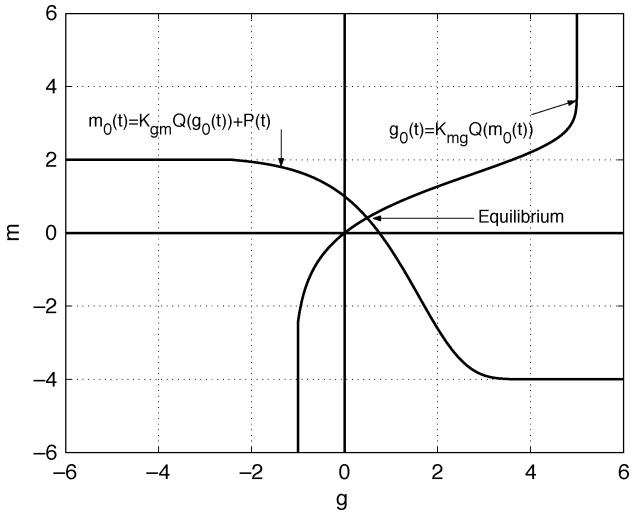

Fig. 4. Equilibrium determined by intersection of nullclines.

Proof: By determining the intersection between the two nullclines in Fig. 4, the proof is trivial. ■

Property 2: With a fixed input P:

a m_1^* is a decreasing function with respect to both K_{mg} and $|K_{gm}|$;

b g_1^* is an increasing function with respect to K_{mg} and a decreasing function with respect to $|K_{gm}|$;

Proof: From property 1, $m_1^* \geq 0$ and $g_1^* \geq 0$, so we have $Q(m_1^*) \geq 0$ and $Q(g_1^*) \geq 0$. Also, $Q'(x) = e^x \cdot e^{-(e^x - 1/Q_m)} \geq 0$. Computing the first-order derivatives from (8), the following are easily proven:

$$\begin{cases} \dfrac{dm_1^*}{dK_{mg}} = \dfrac{-|K_{gm}| \cdot Q(m_1^*) \cdot Q'(g_1^*)}{1 + |K_{mg} \cdot K_{gm}| \cdot Q'(m_1^*) \cdot Q'(g_1^*)} \leq 0 \\ \dfrac{dm_1^*}{d|K_{gm}|} = \dfrac{-Q(g_1^*)}{1 + |K_{mg} \cdot K_{gm}| \cdot Q'(m_1^*) \cdot Q'(g_1^*)} \leq 0 \\ \dfrac{dg_1^*}{dK_{mg}} = \dfrac{Q(m_1^*)}{1 + |K_{mg} \cdot K_{gm}| \cdot Q'(m_1^*) \cdot Q'(g_1^*)} \geq 0 \\ \dfrac{dg_1^*}{d|K_{gm}|} = \dfrac{-K_{mg} \cdot Q(g_1^*) \cdot Q'(m_1^*)}{1 + |K_{mg} \cdot K_{gm}| \cdot Q'(m_1^*) \cdot Q'(g_1^*)} \leq 0 \end{cases} \tag{9}$$

■

A unique equilibrium is a very good property because the system can not have different attractors at the same time. To determine the stability and dynamical behavior, we will investigate the stability of a linearized system of (7) around its equilibrium. The Jacobian matrix of (7) is (see first equation at the bottom of the page) where m_1^* and g_1^* are the fixed point solutions that are determined by K_{mg}, K_{gm} and P. $Q'(x)$ is the derivative of $Q(x)$.

$$A = \begin{bmatrix} 0 & 1 & 0 & 0 \\ -a \cdot b & -(a+b) & a \cdot b \cdot K_{gm} \cdot Q'(g_1^*) & 0 \\ 0 & 0 & 0 & 1 \\ a \cdot b \cdot K_{mg} \cdot Q'(m_1^*) & 0 & -a \cdot b & -(a+b) \end{bmatrix}$$

To calculate the eigenvalues, we have (see second equation at the bottom of the page).

Thus, we obtain

$$[\lambda\cdot(\lambda+a+b)+a\cdot b]^2-(a\cdot b)^2\cdot K_{mg}\cdot K_{gm}\cdot Q'(m_1^*)\cdot Q'(g_1^*)=0.$$

Let $R(K_{mg},K_{gm})=Q'(m_1^*)\cdot Q'(g_1^*)\geq 0$ denote the term related to the equilibrium (thus, also related to the coupling coefficients). We have

$$\lambda\cdot(\lambda+a+b)=-a\cdot b\pm ja\cdot b\cdot\sqrt{|K_{mg}\cdot K_{gm}|\cdot R(K_{mg},K_{gm})}. \tag{10}$$

By solving (10), we obtain the eigenvalues as (see (11) at the bottom of the page).

Let

$$r=\mathrm{Re}\left\{\sqrt{(a-b)^2\pm j4a\cdot b\cdot\sqrt{|K_{mg}\cdot K_{gm}|\cdot R(K_{mg},K_{gm})}}\right\}$$
$$i=\mathrm{Im}\left\{\sqrt{(a-b)^2\pm j4a\cdot b\cdot\sqrt{|K_{mg}\cdot K_{gm}|\cdot R(K_{mg},K_{gm})}}\right\}. \tag{12}$$

It is clear that $r>0$ and $(a+b)>0$. Because $-(a+b)\pm r$ determines the sign of $\mathrm{Re}\{\lambda\}$, we have the following sufficient and necessary conditions for the two equilibrium states that we are interested in:

1) A RKII set (7) has a unique stable equilibrium iff
$$r_{\max}^2<(a+b)^2.$$
2) A RKII set (7) has a unique unstable equilibrium iff
$$r_{\max}^2>(a+b)^2.$$

When $r=(a+b)$, the system is at a bifurcation point. This is the operating point we want to avoid for the purpose of controlling the behavior of a RKII set.

Let $\mathrm{R}_r=(a-b)^2$ and $\mathrm{I}_r=4a\cdot b\cdot\sqrt{|K_{mg}\cdot K_{gm}|\cdot R(K_{mg},K_{gm})}$. Note that

$$\begin{aligned}r_{\max}^2&=\mathrm{Re}^2\left\{\sqrt{\mathrm{R}_r+j\mathrm{I}_r}\right\}\\&=\sqrt{\mathrm{R}_r^2+\mathrm{I}_r^2}\cdot\cos^2\left(\frac{\alpha}{2}\right)\\&=\sqrt{\mathrm{R}_r^2+\mathrm{I}_r^2}\cdot\frac{1+\cos\alpha}{2}\\&=\sqrt{\mathrm{R}_r^2+\mathrm{I}_r^2}\cdot\frac{1+\frac{\mathrm{R}_r}{\sqrt{\mathrm{R}_r^2+\mathrm{I}_r^2}}}{2}\\&=\frac{\sqrt{\mathrm{R}_r^2+\mathrm{I}_r^2}+\mathrm{R}_r}{2}.\end{aligned} \tag{13}$$

By solving $r_{\max}^2=(a+b)^2$, we obtain that the bifurcation occurs when

$$|K_{mg}\cdot K_{gm}|=\frac{1}{Q'(m_1^*)\cdot Q'(g_1^*)}\cdot\frac{(a+b)^2}{a\cdot b}. \tag{14}$$

Under a fixed external input, (14) sets the boundary of stable fixed point solution and limit cycle with respect to the coupling coefficients. Generally, the right side of (14) cannot be explicitly solved. However, the boundary is still easy to find, because only the equilibrium needs to be solved instead of scanning the whole parameter space. In the case of zero input (stable fixed point state), $Q'(m_1^*)\cdot Q'(g_1^*)$ equals to 1. Time constants $1/a$ and $1/b$ are both determined, so we have an explicit upper bound for $|K_{mg}\cdot K_{gm}|$ (a hyperbolic curve in the first quadrant).

In general, with a fixed external input, $|K_{mg}\cdot K_{gm}|$ determines the dynamical behavior of a RKII set by

$$\begin{cases}|K_{mg}\cdot K_{gm}|\\\quad<\frac{1}{Q'(m_1^*)\cdot Q'(g_1^*)}\cdot\frac{(a+b)^2}{a\cdot b} & \text{when } r_{\max}^2<(a+b)^2 \quad (15a)\\|K_{mg}\cdot K_{gm}|\\\quad>\frac{1}{Q'(m_1^*)\cdot Q'(g_1^*)}\cdot\frac{(a+b)^2}{a\cdot b} & \text{when } r_{\max}^2>(a+b)^2. \quad (15b)\end{cases}$$

Theorem 1: The two sufficient and necessary conditions on the coupling coefficients to control the dynamics (i.e., fixed point solution with zero input or limit cycle with positive input) of the system defined by (7) are as follows:

Condition

1) A RKII set stays in an equilibrium state when the input is off (i.e., $P(t)=0$). We require
$$|K_{mg}\cdot K_{gm}|<\frac{(a+b)^2}{a\cdot b}.$$

Condition

2) A RKII set oscillates when the input is on (i.e., $P(t)>0$). We require
$$|K_{mg}\cdot K_{gm}|>\frac{1}{Q'(m_1^*)\cdot Q'(g_1^*)}\cdot\frac{(a+b)^2}{a\cdot b}.$$

Proof: Previous discussions on stability analysis of (7) serve as proofs. ■

Note that the right side of (15b) is also a function of K_{mg} and K_{gm}, so the condition is actually nonlinearly dependent on $|K_{mg}\cdot K_{gm}|$.

$$|\lambda\cdot\mathbf{I}-\mathbf{A}|=\begin{vmatrix}\lambda & -1 & 0 & 0\\ ab & \lambda+(a+b) & -ab\cdot Q'(g_1^*) & 0\\ 0 & 0 & \lambda & -1\\ -ab\cdot Q'(m_1^*) & 0 & ab & \lambda+(a+b)\end{vmatrix}=0.$$

$$\lambda=\frac{-(a+b)\pm\sqrt{(a-b)^2\pm j4a\cdot b\cdot\sqrt{|K_{mg}\cdot K_{gm}|\cdot R(K_{mg},K_{gm})}}}{2}. \tag{11}$$

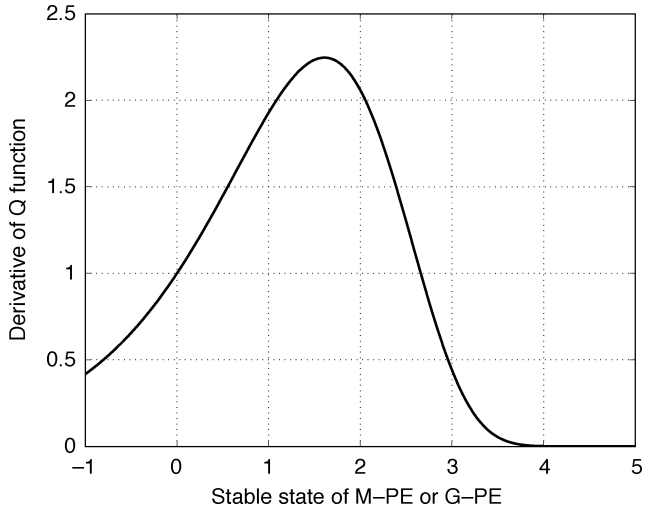

Fig. 5. Derivative of $Q(x)$ when $Q_m = 5$.

Condition 2 also sets restrictions on the value of Q_m in $Q'(x)$. $Q'(x)$ in (14) is the derivative of $Q(x)$ and is defined by

$$Q'(x)\begin{cases} e^x \cdot e^{-\frac{e^x-1}{Q_m}} & x > x_0 \quad (16) \\ 0 & \text{else} \quad (17) \end{cases}$$

where $x_0 = \ln(1 - Q_m \cdot \ln(1 + 1/Q_m))$. Fig. 5 shows a plot of $Q'(x)$. $Q'(x) \geq 0$ and has a maximum value of $Q_m \cdot e^{-(Q_m - 1/Q_m)}$ when $x = \ln(Q_m)$.

To satisfy condition 2, $Q'(x)$ must be greater than 1 for some x. Solving the maximum values, we have $Q_m > 1$. This is in accordance with the requirement in biological models that asymmetry of $Q(x)$ is a necessary source of instability in the neural networks [2].

D. Determining the Right Coupling Coefficients K_{mg} and K_{gm}

Here we provide the specific procedures to choose the right K_{mg} and K_{gm} that satisfy both (15a) and (15b).

1) As in the case when $|K_{mg} \cdot K_{gm}| < ((a+b)^2/a \cdot b)$, the boundary of K_{mg} and K_{gm} is well defined as

$$\begin{cases} K_{mg} > 0 \\ K_{gm} < 0 \\ |K_{mg} \cdot K_{gm}| < \dfrac{(a+b)^2}{a \cdot b}. \end{cases} \quad (18)$$

2) The second case is more complicated because (15b) is nonlinearly related to K_{mg} and K_{gm}. Although we could not calculate an analytical solution of the region where a valid K_{mg} and K_{gm} exist, we will show how to determine an approximate region. Again, the equilibrium is determined by

$$\begin{cases} -ab \cdot m_1^* + ab \cdot (K_{gm} Q(g_1^*) + P) = 0 \\ -ab \cdot g_1^* + ab \cdot K_{mg} Q(m_1^*) = 0 \end{cases}$$

where m_1^* and g_1^* are the fixed point solutions.

Solving the above equations and substituting $Q'(x)$ with $Q(x)$, the boundary of Condition 2 (i.e., $|K_{mg} \cdot K_{gm}| = 1/(Q'(m_1^*) \cdot Q'(g_1^*)) \cdot (a+b)^2/a \cdot b$) could also be defined as

$$\begin{aligned} &|K_{mg} \cdot K_{gm}| \cdot R(K_{mg}, K_{gm}) \\ &\quad = |K_{mg} \cdot K_{gm}| \cdot Q'(m_1^*) \cdot Q'(g_1^*) \\ &\quad = |K_{mg} \cdot K_{gm}| \cdot e^{m_1^* + g_1^*} \cdot \left(1 - \frac{g_1^*}{Q_m \cdot K_{mg}}\right) \\ &\qquad \cdot \left(1 - \frac{P - m_1^*}{Q_m \cdot |K_{gm}|}\right) \\ &\quad = e^{m_1^* + g_1^*} \cdot \left(K_{mg} - \frac{g_1^*}{Q_m}\right) \cdot \left(|K_{gm}| - \frac{P - m_1^*}{Q_m}\right) \\ &\quad = \frac{(a+b)^2}{a \cdot b} \end{aligned} \quad (19)$$

where $m_1^*(> 0)$ and $g_1^*(> 0)$ are also functions of K_{mg} and K_{gm}. It is hard to find an explicit solution for the lower bound of the desired K_{mg} and K_{gm}, especially in the form of $|K_{mg} \cdot K_{gm}|$. However, we can still find ways to determine a subset of the desired regions. The following properties obtained from (19) guide us in finding the appropriate coupling coefficients.

Property 3: Given $m_1^* > 0$ and $g_1^* > 0$, if

$$Q'(m_1^*) \cdot Q'(g_1^*) = Q'(m_1^*) \cdot Q'(K_{mg} \cdot Q(m_1^*)) = 1,$$

then

$$Q'(m_1^*) \cdot Q'(K_{mg} \cdot Q(m_1^*)) \geq 1$$

for all $0 \leq m_1 \leq m_1^*$.

Proof: $Q'(m_1^*) \cdot Q'(K_{mg} \cdot Q(m_1^*))$ has similar shape as $Q'(x)$, So it has a lower bound of 1 when m_1^* decreases. ■

Property 4: Suppose that K_{mg}^* and K_{gm}^* is a set of values that satisfy both conditions. If we fix the value of $K_{mg} = K_{mg}^*$ and increase K_{gm} until $|K_{mg}^* \cdot K_{gm}| = (a+b)^2/a \cdot b$, then $|K_{mg}^* \cdot K_{gm}| > (1/(Q'(m_1^*) \cdot Q'(g_1^*))) \cdot (a+b)^2/a \cdot b$ is automatically satisfied

Proof: At the point where $|K_{mg}^* \cdot K_{gm}^*| > (1/(Q'(m_1^*) \cdot Q'(g_1^*))) \cdot (a+b)^2/a \cdot b$, we have $Q'(m_1^*) \cdot Q'(g_1^*) > 1$. Increasing K_{gm}, both m_1^* and g_1^* are decreased (Properties 1). According to Properties 3, $Q'(m_1^*) \cdot Q'(g_1^*) > 1$ is also true when $|K_{mg}^* \cdot K_{gm}|$ is increased to $(a+b)^2/a \cdot b$. Thus

$$\left|K_{mg}^* \cdot K_{gm}\right| = \frac{(a+b)^2}{a \cdot b} > \frac{1}{Q'(m_1^*) \cdot Q'(g_1^*)} \cdot \frac{(a+b)^2}{a \cdot b}$$

is automatically satisfied. ■

Based on the above properties and because (19) is a continuous function, we can start from $|K_{mg} \cdot K_{gm}| = (a+b)^2/a \cdot b$, then fix the value of K_{mg}, decrease the value of $|K_{gm}|$ slightly, and apply a positive external input to satisfy both Condition 1 and Condition 2. The first term in (19) will be exponentially increasing while the other two terms will be linearly decreasing with respect to an increase of m_1^* and g_1^*. If we keep decreasing $|K_{gm}|$, two cases can possibly occur. $|K_{mg} \cdot K_{gm}|$ drops until Condition 2 is not satisfied. Or, it will reach another bifurcation point before that. Similarly, starting from $|K_{mg} \cdot K_{gm}| = (1/(Q'(m_1^*) \cdot Q'(g_1^*))) \cdot (a+b)^2/a \cdot b$ and increasing only the

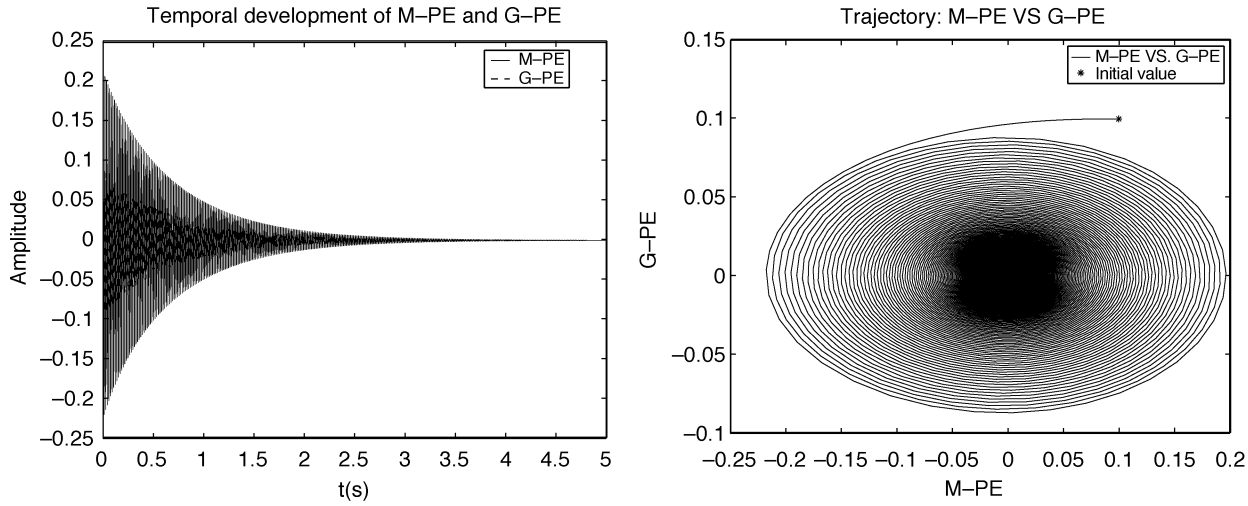

(a) (b)

Fig. 6. Temporal development of M-PE and G-PE: fixed point state. External input $P = 0$. Product of coupling coefficients $|K_{mg} \cdot K_{gm}| = 5.5$ while $K_{mg} = 1$ and $|K_{gm}| = 5.5$. Starting from initial conditions $m_1(t_0) = 0.1$ and $g_1(t_0) = 0.1$, the RKII set converges to a stable fixed point at (0,0). (a) Temporal development of M-PE and G-PE. (b)Phase plot.

value of $|K_{gm}|$ will also provide a range of valid values. However, there is no guarantee that these two areas overlap. Nevertheless, experiments show that for reasonable and normally used parameters (such as the a and b given previously, and $Q_m = 5$), we can use the above procedures as a rule of thumb to easily determine in which direction to change the invalid values and reach the desired ones.

E. Dynamics Controlled by an External Input

The state of a RKII set is controlled by an external stimulus P. Here, P is a time-invariant input with two states: *off* and *on*. *Off* state $(P = 0)$ is guaranteed by Condition 1 to be stable. However, not every positive value (*on*) could induce the oscillatory state in a RKII set. We will see in the following that P creates oscillatory behavior only in a bounded region.

Property 5: In the system defined by (7), the fixed point solutions m_1^* and g_1^* are both monotonically increasing functions with respect to the external input P.

Proof: The first-order derivatives of m_1^* and g_1^* with respect to P are

$$\frac{dm_1^*}{dP} = \frac{1}{1 + |K_{mg} \cdot K_{gm}| \cdot Q'(m_1^*) \cdot Q'(g_1^*)} > 0$$
$$\frac{dg_1^*}{dP} = \frac{K_{mg} \cdot Q'(m_1^*)}{1 + |K_{mg} \cdot K_{gm}| \cdot Q'(m_1^*) \cdot Q'(g_1^*)} > 0. \quad (20)$$

Recall that $K_{mg} > 0$ and $Q'(x) \geq 0$. So both derivatives in (20) are positive. m_1^* and g_1^* are both monotonically increasing functions with respect to the external input P. ■

Theorem 2: Given a set of fixed coupling coefficients K_{mg} and K_{gm}, the values of external input P that enable oscillatory state in a RKII set only exist in a bounded region.

Proof: According to Condition 2 and the properties of $Q'(x)$, we have

$$\frac{(a+b)^2}{a \cdot b} \cdot \frac{1}{|K_{mg} \cdot K_{gm}|} < Q'(m_1^*(P)) \cdot Q'(g_1^*(P)) < \left(Q_m \cdot e^{-\frac{Q_m - 1}{Q_m}}\right)^2.$$

Thus, both m_1^* and g_1^* are bounded. According to Property 5, P must be bounded. ■

III. Experimental Results

A. Control of RKII Dynamics by the Coupling Coefficients

We will give two examples in which the external input is fixed to either zero or a positive value. In the case of zero input, an exact boundary is shown.

1) When $P(t) = 0$, (15a) gives a fixed bifurcation boundary that divides the space into areas of oscillation and fixed point solutions. As given in [1], $a = 220/s$ and $b = 720/s$. So we have

a) $|K_{mg} \cdot K_{gm}| < 5.5783$: A RKII set is stable and has a fixed point solution of (0,0);

b) $|K_{mg} \cdot K_{gm}| > 5.5783$: A RKII set oscillates.

Note that in this case, the actual values of K_{mg} and K_{gm} do not change the qualitative behavior as long as $|K_{mg} \cdot K_{gm}|$ is unchanged. In the examples, K_{mg} is fixed to one and K_{gm} will be changed to different values of $|K_{mg} \cdot K_{gm}|$. In Fig. 6, when $K_{mg} = 1$ and $K_{gm} = -5.5$ the output goes to a fixed point with a very long transient time. When we increase $|K_{gm}|$ to 5.6, the output presents an oscillatory state (Fig. 7).

2) In the second example, we set the input to $P(t) = 1$. As discussed in the previous section, there is no explicit expression of a lower bound in $|K_{mg} \cdot K_{gm}|$ but once we determine one set of valid values, all other values with a larger $|K_{gm}|$ are all possible choices to keep the system oscillating with a positive external input. Again, we will set K_{mg} to 1. Fig. 8 shows the transient output of M-PE and G-PE with a value of $K_{gm} = -4$. Apparently, the coupling strength is not large enough to produce an oscillating system. The system has a equilibrium at (0.1776, 0.1906) and

$$|K_{mg} \cdot K_{gm}| = 4 < \frac{1}{Q'(m_1^*) \cdot Q'(g_1^*)} \cdot \frac{(a+b)^2}{a \cdot b} = 4.1852.$$

Trying another $K_{gm} = -5$, we have an oscillatory state, as shown in Fig. 9. In this case, the equilibrium with decreased

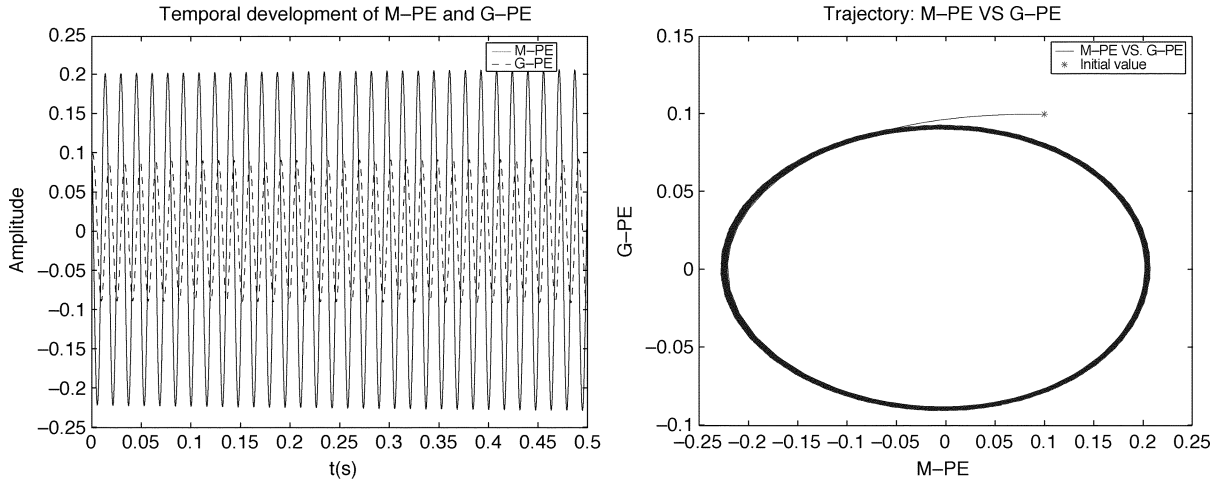

(a) (b)

Fig. 7. Temporal development of M-PE and G-PE: oscillatory state. External input $P = 0$. Product of coupling coefficients $|K_{mg} \cdot K_{gm}| = 5.6$ while $K_{mg} = 1$ and $|K_{gm}| = 5.6$. Starting from initial conditions $m_1(t_0) = 0.1$ and $g_1(t_0) = 0.1$, the RKII set converges to a stable limit cycle. (a) Temporal development of M-PE and G-PE. (b) Phase plot.

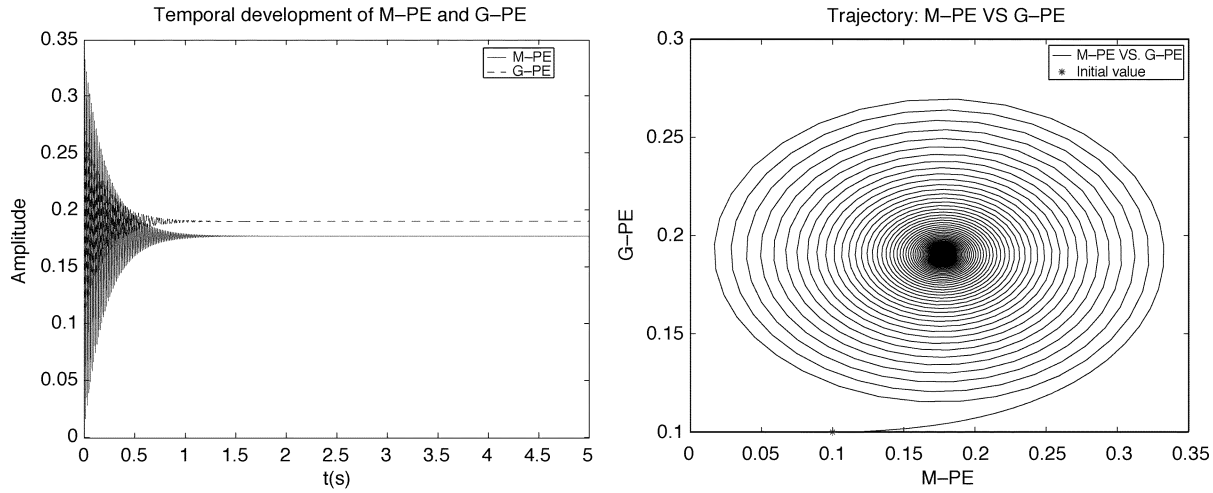

(a) (b)

Fig. 8. Temporal development of M-PE and G-PE: fixed point state. External input $P = 1$. Product of coupling coefficients $|K_{mg} \cdot K_{gm}| = 4$ while $K_{mg} = 1$ and $|K_{gm}| = 4$. Starting from initial conditions $m_1(t_0) = 0.1$ and $g_1(t_0) = 0.1$, the RKII set converges to a stable fixed point at (0,0). (a) Temporal development of M-PE and G-PE. (b)Phase plot.

values of m_1^* and g_1^* is at (0.1502,0.1595) and condition 2 is satisfied

$$|K_{mg} \cdot K_{gm}| = 5 > \frac{1}{Q'(m_1^*) \cdot Q'(g_1^*)} \cdot \frac{(a+b)^2}{a \cdot b} = 4.3762.$$

After scanning different value of K_{gm}, we obtained an approximate minimum value 4.237 as the lower bound. So, in this case, $K_{mg} = 1$ and $-5.5783 < K_{gm} < -4.237$ are possible solutions to achieve the desired dynamical behavior in a RKII set. Note that, with a relative small $|K_{gm}|$, the amplitude of the oscillation will be very small and the transient time to reach a stable limit cycle is rather large. So, normally, a large enough $|K_{gm}|$ is desired.

B. Controlling a RKII Set by the External Input

To show that a valid stimulus to the system only exists in a bounded region of P, we fix $K_{mg} = 1$ and $|K_{gm}| = 5$ and scan different values of P. Approximately, with this set of coupling coefficients, P must be in the region (0.42, 26.06) to effectively make the RKII set oscillating. Fig. 10 shows the transient signal of the system with two different P values: 0.35 and 26.1. We see that, even in the positive region, P should neither be too small nor too large to satisfy condition 2

$$\begin{cases} |K_{mg} \cdot K_{gm}| = 5 < \frac{1}{Q'(m_1^*) \cdot Q'(g_1^*)} \\ \quad \cdot \frac{(a+b)^2}{a \cdot b} = 5.0974 & \text{when } P = 0.35 \\ |K_{mg} \cdot K_{gm}| = 5 < \frac{1}{Q'(m_1^*) \cdot Q'(g_1^*)} \\ \quad \cdot \frac{(a+b)^2}{a \cdot b} = 5.2395 & \text{when } P = 26.1. \end{cases}$$

C. Parameter Space

We scanned the space of K_{mg} and K_{gm} to provide a sense of the shape of the boundaries (Fig. 11). The result is under the conditions $P = 1$ and $Q_m = 5$. We see that in the scanned ranges, the lower bound follows the properties we discussed in Section II-D. If an arbitrarily determined c oupling coefficient

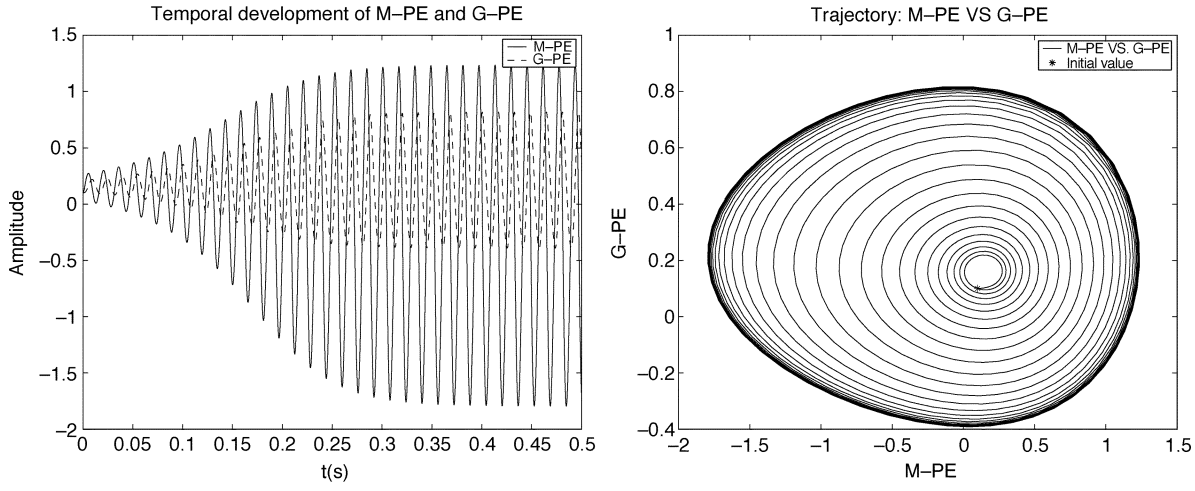

Fig. 9. Temporal development of M-PE and G-PE: oscillatory state. External input $P = 1$. Product of coupling coefficients $|K_{mg} \cdot K_{gm}| = 5$ while $K_{mg} = 1$ and $|K_{gm}| = 5$. With stronger coupling, starting from initial conditions $m_1(t_0) = 0.1$ and $g_1(t_0) = 0.1$, the RKII set oscillates and converges to a stable limit cycle under a positive external input. (a) Temporal development of M-PE and G-PE. (b) Phase plot.

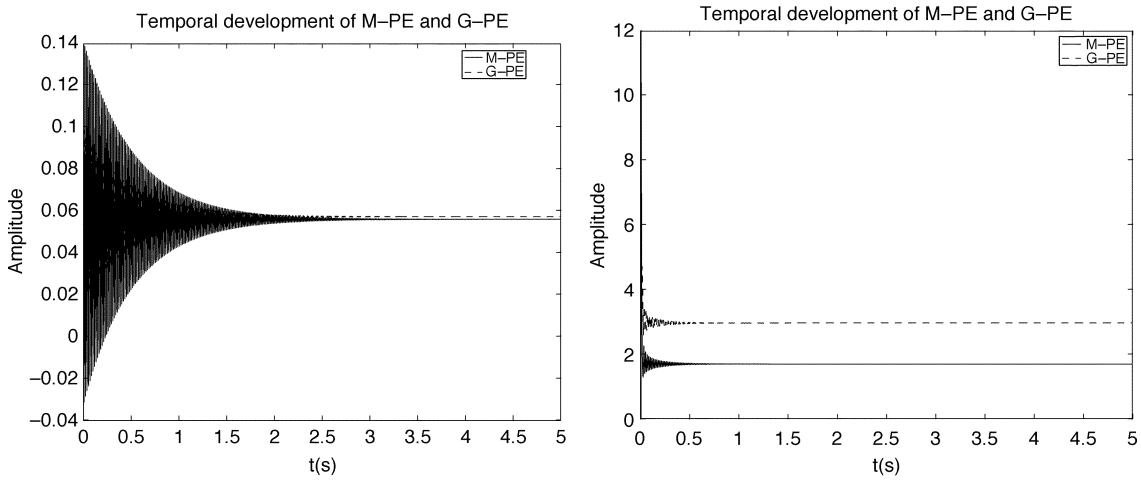

Fig. 10. Temporal development of M-PE and G-PE: fixed point state. Product of coupling coefficients $|K_{mg} \cdot K_{gm}| = 5$ while $K_{mg} = 1$ and $|K_{gm}| = 5$. Starting from initial conditions $m_1(t_0) = 0.1$ and $g_1(t_0) = 0.1$, the RKII set converges to a stable fixed point even with positive inputs. (a) Temporal development of M-PE and G-PE. External input $P = 0.35$. (b) Temporal development of M-PE and G-PE. External input $P = 26.1$.

can not make the RKII set controllable as expected, we just need to increase the value of $|K_{gm}|$, while keeping K_{mg} unchanged.

IV. Conclusion

We presented a dynamical analysis of a RKII set behavior. The main purpose is to find the desired regions in the parameter space of the coupling coefficients K_{mg} and K_{gm} so that the RKII set is totally controllable, that is, it displays the desired behavior of collapsing to a fixed point with no input and oscillating when driven by a positive input. In the first case, the product of the two coupling coefficients determines whether the stability conditions are satisfied. In the second case, there is no analytical solution for the conditions on the coupling coefficients. However, we provided a systematic way to easily locate the appropriate values of K_{mg} and K_{gm}. The effect of the amplitude of time-invariant input P on the dynamics of the system is also discussed. Results show that the input should be limited to a bounded region for robust control of the RKII set.

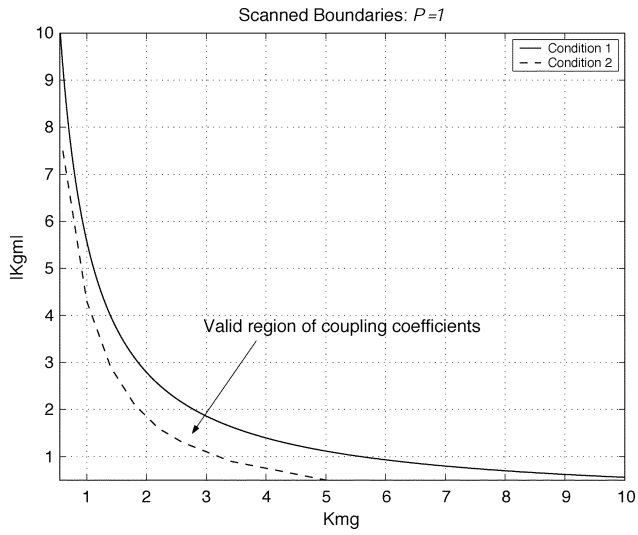

Fig. 11. Scanned parameter space of $|K_{mg} \cdot K_{gm}|$.

The analysis contained in this paper already leads us to select appropriate parameters in the design of analog VLSI components to implement the olfactory cortex dynamics. Here the problem is that the designed parameters suffer variations due to fabrication, so the goal is to select them at values that have the largest tolerance. This analysis is also helpful to continue the goal of understanding higher lever structures (KII and KIII networks) that form the computational model of the olfactory system. The specified system properties can also help us determine where and how to utilize the system for various real time applications.

REFERENCES

[1] W. Freeman, *Mass Action in the Nervous System*. New York: Academic, 1975.

[2] J. Principe, V. Tavares, J. Harris, and W. Freeman, "Design and implementation of a biologically realistic olfactory cortex in analog VLSI," *Proc. IEEE*, vol. 89, no. 7, pp. 569–571, July 2001.

[3] R. Llinas, *I of the Vortex: From Neurons to Self*. Cambridge, MA: MIT Press, 2001.

[4] S. Kelso, *Dynamic Patterns: The Self-Organization of Brain and Behavior*. Cambridge, MA: MIT Press, 1995.

[5] V. Tavares, "Design and implementation of a biologically realistic olfactory cortex model," Ph.D. dissertation, Univ. of Florida, Gainesville, FL, May 2001.

[6] S. Grossberg, "Pattern learning by functional-differential neural networks with arbitrary path weights," in *Delay and Functional Differential Equations and Their Applications*, S. Schmitt, Ed. New York: Academic, 1972, pp. 121–160.

[7] J. Hopfield, "Neurons with graded response have collective computational properties like those of two-state neurons," *Proc. Nat. Acad. Sci.*, vol. 81, pp. 3088–3092, 1984.

[8] D. Kaplan and L. Glass, *Understanding Nonlinear Dynamics*. New York: Springer-Verlag, 1995.

[9] Y. Yao, W. Freeman, B. Burke, and Q. Yang, "Pattern recognition by a distributed neural network: an industrial application," *Neural Netw.*, vol. 4, no. 1, pp. 103–121, 2001.

[10] R. Kozma and W. Freeman, "Chaotic resonance-methods and applications for robust classification of noisy and variable patterns," *Int. J. Bifurcation Chaos*, vol. 11, no. 6, pp. 1607–1629, 2001.

[11] W. Freeman and S. Jakubith, "Bifurcation analysis of continuous time dynamics of oscillatory neural networks," in *Brain Theory-Spatio-Temporal Aspects of Brain Function*, A. Aertsen and W. von Seelen, Eds. Amsterdam, The Netherlands: Elsevier, 1993, pp. 183–208.

[12] F. Hoppensteadt, *Analysis and Simulation of Chaotic Systems*, 2nd ed. New York: Springer-Verlag, 2000.

[13] Y. Kuznetsov, L. Kuznetsov, and J. Marsden, *Elements of Applied Bifurcation Theory*, 2nd ed. New York: Springer-Verlag, 1998.

[14] W. D. Jordan and P. Smith, *Nonlinear Ordinary Differential Equations*, 2nd ed. Oxford, U.K.: Clarendon, 1987.

[15] J. Palis Jr. and W. de Melo, *Geometric Theory of Dynamical Systems*. New York: Springer-Verlag, 1982.

Dongming Xu (S'04) received the B.E. degree in electrical engineering from Xi'an Jiaotong University, China, in 1999 and the M.S. degree in electrical engineering from the University of Florida, Gainesville, in 2001. He is currently working toward the Ph.D. degree at the University of Florida.

Since 1999, he has been a Research Assistant in the Computational NeuroEngineering Laboratory (CNEL), University of Florida. His research interests include nonlinear dynamical systems for information processing, analog VLSI design, and information theory.

José C. Principe (M'83–SM'90–F'00) is Distinguished Professor of Electrical and Biomedical Engineering at the University of Florida, Gainesville, where he teaches advanced signal processing and artificial neural networks (ANN's) modeling. He is BellSouth Professor and Founder and Director of the University of Florida Computational NeuroEngineering Laboratory (CNEL). He has been involved in biomedical signal processing, in particular the electroencephalogram (EEG), and the modeling and applications of adaptive systems. He has more than 100 publications in refereed journals, 10 book chapters, and over 200 conference papers.

Dr. Principe is Editor in Chief IEEE TRANSACTIONS ON BIOMEDICAL ENGINEERING, President Elect of the International Neural Network Society, and formal Secretary of the Technical Committee on Neural Networks of the IEEE Signal Processing Society. He is also a member of the Scientific Board of the Food and Drug Administration, and a member of the Advisory Board of the University of Florida Brain Institute.